Microbiome disturbance and resilience dynamics of the upper respiratory tract in response to influenza A virus infection in analog hosts

Drishti Kaul[1,8], Raveen Rathnasinghe[2,8], Marcela Ferres[2], Gene S. Tan[1,3], Aldo Barrera[2,4], Brett E. Pickett[5], Barbara A. Methe[5a], Suman Das[5], Isolda Budnik[2], Rebecca A. Halpin[5], David Wentworth[5b], Mirco Schmolke[6c], Ignacio Mena[6], Randy A. Albrecht[6], Indresh Singh[5], Karen E. Nelson[5], Adolfo García-Sastre[6,7], Chris L. Dupont[1*], Rafael A. Medina[2,4,6*].

[1]J. Craig Venter Institute, 4120 Capricorn Lane, La Jolla, CA 92037, USA.

[2]Departmento de Enfermedades Infecciosas e Inmunología Pediátrica, Facultad de Medicina, Pontificia Universidad Católica de Chile, Santiago, Chile.

[3] Department of Infectious Diseases, University of California San Diego, La Jolla, CA 92037, USA

[4]Millennium Institute on Immunology and Immunotherapy, Santiago, Chile

[5]J. Craig Venter Institute, 9704 Medical Center Drive, Rockville, Maryland 20850, 14 USA.

[6]Department of Microbiology, Global Health and Emerging Pathogens Institute, Icahn School of Medicine at Mount Sinai, New York, NY 10029, USA.

[7]Department of Medicine, Icahn School of Medicine at Mount Sinai, New York, NY 10029, USA.

[8]These authors contributed equally to this work

[a] University of Pittsburgh, Department of Medicine, Pittsburgh PA 15213

[b] Present address: National Center for Immunization and Respiratory Diseases, Centers for Disease Control and Prevention, Atlanta, GA, USA.

[c] Present address: Department of Microbiology and Molecular Medicine, University of Geneva, Switzerland

*Corresponding author: E-mail: rmedinas@med.puc.cl , cdupont@jcvi.org

Summary

Infection with influenza can be exacerbated by bacterial co-infections, which often results in disease exacerbation because of host responses and cellular damage. The native microbiome likely plays a role, yet the effects of influenza infection on the upper respiratory tract (URT) microbiome are largely unknown. We performed a longitudinal study to assess temporal dynamics of the URT microbiomes of uninfected and influenza virus-infected humans and ferrets. Uninfected human patients and ferret URT microbiomes had stable "heathy ecostate" communities both within and between individuals. In contrast, infected patients and ferrets exhibited large changes in bacterial community composition over time and between individuals. "Non-healthy" ecostates of infected individuals progressed towards the "healthy ecostate" over time, coinciding with viral clearance. Blooms of *Pseudomonas* were a statistically associated constant in the disturbed microbiomes. The dynamic and resilient nature of the microbiome during influenza virus infection in multiple hosts provides a potential therapeutic target.

Keywords: Influenza A virus, resilience, biodiversity, microbiome, upper respiratory tract, H1N1, H3N2, ecostate, ferrets, humans

Introduction

Influenza is a highly infectious upper respiratory tract (URT) disease in humans caused by a negative-sense segmented RNA virus. Frequent point mutations on the hemagglutinin and neuraminidase glycoproteins on the surfaces of influenza A virus (IAV) particles (antigenic drift) contribute to the constant need for updated influenza virus vaccines. This evolutionary arms race between vaccine design and viral mutation contributes to annual influenza epidemics worldwide, which on average results in 3 to 5 million cases of severe illness and up to 291,000 to 646,000 deaths annually (Iuliano et al., 2017). The modular architecture of the segmented IAV genome allows for genetic re-assortment (antigenic shift) with other divergent influenza viruses, resulting in the sporadic emergence of novel influenza viruses capable of

causing large epidemics or pandemics. Circulation of a new IAV in the naïve human population has caused pandemics in the past resulting in significant morbidity and mortality, the most notable in 1918 and 1919, when the *Spanish flu* killed approximately 20 to 50 million people worldwide (Johnson and Mueller, 2002). Retrospective analyses of autopsy specimens from the *1918* pandemic revealed the prevalence of secondary superinfection caused by URT bacteria (Brundage, 2006; Brundage and Shanks, 2008; Morens et al., 2008). However, the role of bacterial co-infection in disease prognosis is not only confined to pandemics; bacterial and virus co-infection during seasonal influenza epidemics are commonly associated with increase hospital admissions, severe disease and deaths (Blyth et al., 2013; Shah et al., 2016).

Nonetheless, infection with influenza virus alone is recognized as a public health concern contributing to significant disease and economic burden in both humans and animals. The exact mechanisms by which prior infection with influenza virus increase susceptibility to a secondary bacterial infection have not been determined. Additionally, the effects of influenza virus replication on the human or animal microbiome during infection have yet to be elucidated on a community wide scale. Although the microbiome of non-diseased individuals is relatively stable, influenza virus infection has been shown to increase the diversity of bacterial taxa that are present in the URT (Charlson et al., 2011). Specifically, IAV appears to cause changes in the relative abundances of *Staphylococcus* and *Bacteroides* genera (Tarabichi et al., 2015), as well as *Haemophilus*, *Fusobacteria*, and other taxa (Langevin et al., 2017). Temporary disturbances to the microbiome due to the changes in the local epithelia during acute or chronic conditions has also been reported as a predisposing factor for infections (Gao et al., 2014; Huang and Lynch, 2011; Planet et al., 2016; Whelan et al., 2014).

The observed diversity in the URT microbiome, together with its role in immunity and susceptibility to pathogens has been studied previously (Chaban et al., 2013; Gao et al., 2014; Ichinohe et al., 2011). Other studies have reported that the URT microbiome also plays a role in modulating the inflammatory response that is generally present during infection with influenza A virus (Ichinohe et al., 2011; Wang et al., 2013). In addition, the intestinal microbiome composition has been shown to regulate the toll-like receptor 7 signaling pathway following infection with IAV (Wu et al., 2013). Nonetheless, the effect of IAV replication

and induction of innate immune response on the composition of the URT microbiome is still largely unexplored.

In addition to sharing similar lung physiology, both humans and ferrets are known to be susceptible to the same strains of the influenza virus [18, 19](Belser et al., 2016; Belser et al., 2011). Therefore, this may be an ideal model system to assess the composition and temporal dynamics of the microbiome in response to IAV infection. The similarity between the ferret and human URT microbiome in terms of composition and temporal dynamics is unknown. In this study, we examined the longitudinal diversity of the URT microbiome of influenza infected and uninfected human cohorts, as well as control uninfected and experimentally infected ferrets. These experiments verified consistencies in microbiome dynamics between the two host systems and suggest that microbiome disturbance and resilience dynamics may be critical to addressing the bacterial co-infections associated with influenza-derived morbidity.

Results

Influenza virus infection modulates the microbiome structure of the URT in ferrets

To determine if IAV infection influences the URT microbiome, we designed a longitudinal study to obtain nasal wash samples from ferrets infected with IAV. Our goal was to assess and compare the temporal microbiome biodiversity in response to infection as ecological disturbances of the URT caused by viral infection. We used the well-established ferret model of IAV infection to collect nasal washes from 7 uninfected ferrets and 7 ferrets infected with the A/Netherlands/602/2009 (H1N1) pandemic strain, at 0, 1, 3, 5, 7 and 14 dpi.

The dynamics and relative abundances of bacteria in the URT microbiome were examined by pyrosequencing of the V1-V3 region of the 16S rRNA. A total of 649,440 reads clustered into 259 operational taxonomic units (OTUs) with 79% of reads mapping (Table 1). The count abundance data for the OTUs was normalized to account for the sampling process and the library size as a confounding factor for the beta-diversity analyses. Additionally, OTUs with counts less than 5 were removed to avoid inflating the importance of any contaminant sequences that might be present in the data. Principal Coordinates Analysis (PCoA) of beta diversity between the healthy and influenza infected cohorts in three dimensions

demonstrated variability consistent with influenza perturbing and modulating the microbiome structure (Fig. 1). Infection status strongly influenced the ordination of the samples as measured by the Bray-Curtis beta-diversity metric (R=0.503, p-value < 0.001). The IAV-negative (blue) and IAV-positive (red) ferret microbial communities clustered separately, while samples from the IAV infected animals show divergence from each other (Fig. 1). By the final time point, Day 14 (cyan), the microbiome of infected ferrets was more similar to the Day 0 samples (lavender) and those of the uninfected controls (blue).

Quantitative metrics of diversity were used to compare the microbiomes of influenza infected and control ferrets and humans. Beta diversity distance analyses (Figure S1) demonstrated ferret microbiomes had higher diversity between infection states than within them. Student's two sample two-sided t-tests confirmed that the diversity between the two states (infected and uninfected) was statistically significant, with the microbiomes of infected ferrets being more diverse (Table S1). The t-statistic for the "All within infection" versus "All between infection" of -29.1592 corresponds to a Bonferroni-corrected parametric p-value of 1.90e-166 (Table S1). The PCoA and statistical analyses show that infected ferrets have a far more dynamic URT microbiome than that of the uninfected group.

Temporal changes in the structure of the ferret URT microbiome during and after IAV infection

To assess the correlation of clinical symptoms overtime during acute IAV infection, we monitored the body weight of all ferrets from 0 to 14 dpi, which demonstrated a clear weight loss among the infected animals (Fig. 2A). As expected, the maximum weight loss concurred with with peak IAV titer at 3 to 5 days after viral inoculation, and recovery in body weight correlated with the lack of detectable virus after day 7 (Fig. 2B). To visualize the temporal trajectory of the ferret microbiome, the community composition for one representative influenza-infected and one uninfected ferret (ferret_595 and ferret_592 respectively) were examined with regards to their taxonomic profiles across six different time points (Fig. 2C and 2D). At the order level, we observed that in influenza-infected ferrets, *Pseudomonadales* (pink) blooms during the earlier time points (days 5 and 7, Fig. 2C-F) correlated with maximal weight loss and peak viral titers (Fig. 2A and B). A few of the less-abundant phyla included *Actinobacteria* and *Firmicutes* (Fig. S2). We observed that the abundance of *Pseudomonas* decreased over time in the infected ferrets, reaching the basal

abundance found in healthy ferrets 14 days post infection (dpi). For the uninfected ferrets, the microbiomes were more stable and *Clostridiales* (dark blue) was the most abundant taxonomic group, followed by *Lactobacillales* (light blue). *Pseudomonadales* was among the least abundant taxonomic group in the uninfected controls (Fig. 2D). These results demonstrate that IAV infection induces a dynamic modulation of the microbiome structure in the URT of ferrets, which correlated with viral replication and pathogenesis. However, our data suggests that basal level could be reestablished upon viral clearance.

IAV infection differentiates the ferret URT microbiome structure into defined ecostates

Due to the dynamic nature of the ferret URT microbiome during IAV infection, we hypothesized that infection perturbs the microbiome structure resulting in distinct signature microbiomes that differentiate infected from uninfected ferrets. Thus, we used Infinite Dirichlet-multinomial Mixture Model (iDMM)(O'Brien et al., 2016), which is an extension of the Dirichlet-multinomial mixture model (DMM)(Holmes et al., 2012) that has been shown to help understand and interpret taxon abundance data. This is an un-supervised clustering method that applies Bayesian statistics to quantitatively assess the data and accurately capture the features that are present. Essentially, given a set of subsampled distributions, the iDMM model predicts the original number of full-size distributions together with their composition. The model recognizes the noise inherent in our extreme subsampling and accounts for it through the examination of distributions (samples) over distributions (OTUs). The nonparametric nature of the iDMM model makes it ideal for understanding complex ecological data where the original number of the sampled communities, known as ecostates, is unknown, as observed for the datasets in this study. The iDMM model was run over 1000 iterations, which collapsed the data into two ecostates. The mean of the likelihood ratio at each iteration converged 70 iterations into the analysis, splitting into two ecostates until the last iteration. One of the two ecostates was comprised of all the uninfected data points (or the “healthy” ecostate) while the other contained most of the influenza infected data points (the “unhealthy” ecostate, Table 2). There were notable exceptions; despite the perturbation caused by the infection, all Day 14 samples in the infected cohort moved from the “unhealthy” ecostate to the “healthy” ecostate, which is also shown in the ordination plot in Fig 1. Moreover, the healthy ecostate also contained a few of the earlier data points (Day 0 and Day 1) of the influenza-

infected cohort, indicating a temporal lag in changes to the ferret microbiome at those timepoints when the titer was submaximal (Fig. 2B)

165 We also identified a diagnostic OTU for each of these ecostates, which is the OTU with the highest posterior predictive probability in the ecostate and therefore drives the clustering. The iDMM analysis predicted the diagnostic OTU for the "unhealthy" ecostate to be Otu000004 which belongs to the *Pseudomonadales* order, with a posterior predictive probability of 0.11 (Table 2), followed by Otu000003 which also belonged to the *Pseudomonas* genus. This is consistent with the qualitative taxonomic profiling shown in Fig. 2. As
170 for the "healthy" ecostate, Otu000001, which belongs to the *Clostridia* family, was the diagnostic OTU with a posterior predictive probability of 0.20 (Table 2). The posterior probabilities for each taxon were calculated within each sample by observing the fraction of simulated samples with more counts than the observed value. The probabilities associated with the diagnostic OTUs can be thought in terms of being relative to all taxa present. Interestingly, the diagnostic OTUs for both ecostates are among the ten most abundant OTUs
175 for the data (Fig. S2).

In parallel, we employed a random forest analysis to identify predictive features in the data. The method we developed iterates through unique random forest models (each seeded with a different random state) and attempts to fit the model to a random subset of the data with five samples removed from the training set, as described in the Methods. If the model could accurately predict all five of the left-out samples during
180 the cross-validation step, then its feature importance vector (mean decrease gini index) including weights for every OTU's predictive capacity was collected. The results from the random forest analysis aligned well with the iDMM diagnostic OTU prediction in that Otu000004 (*Pseudomonadales*) was the most predictive attribute for the influenza infected samples, followed by Otu000028 (*Enterobacteriaceae*) and Otu000017 (*Bacillales*), with a maximum accuracy of 96% (Table S2). Altogether, IAV infection results in a nasal bloom
185 of multiple *Pseudomonadales* in the ferrets, displacing the *Clostridia* associated with the "healthy" and stable ecostate.

Effects of influenza on URT microbiome dynamics in human clinical samples

In order to determine how the human microbiome structure is modulated by the IAV infection, we established a human cohort study and obtained nasopharyngeal swabs at multiple time points after the

190 initial influenza-prompted hospital visits (days 1 to 22) from 30 human subjects recruited during 2011 and 2012. As healthy controls, we included nasal swab samples taken at 6 time points (days 1, 2, 3, 5, 7 and 28) from 22 healthy human subjects free of any respiratory infections (Table S3). We hypothesized that IAV infection in humans will result in the clustering of microbiomes according to infection status, as observed in the ferret experiment. The 16S amplicon sequencing yielded a total of 2.3 million sequences, which were
195 then clustered into 707 OTUs (Table 1) using similar thresholds for length and expected error as were chosen for the ferret data. Over 90% of the reads mapped back to the OTUs (Table 1). As before, the count abundance data for the OTUs was normalized and the low abundance taxa were filtered out from the count data. Metric multidimensional scaling of the beta diversity explains 38.5% of the variability across the first three components (Fig. 3). Similar to the ferret experiments, the plot shows that the infection status has a
200 strong influence on the ordination of the samples, as measured by the Bray-Curtis metric ($R=0.649$, p-value < 0.001). The uninfected (blue) and infected (red indicates data points with positive qPCR detection for the influenza virus and yellow indicates data points from symptomatic individuals that were below the qPCR detection limits) communities cluster away from each other (Fig. 3). The microbiome for the IAV-infected cohort is more dynamic than that of the uninfected IAV-free cohort, validating of the "Anna Karenina"
205 principle of microbiomes, which refers to the notion that there is much more variability in the microbial communities of dysbiotic individuals than in healthy ones. Quantitative examinations revealed that the range for infection-associated beta diversity is much lower in the ferret samples than it is from human clinical samples. As observed in the ferrets, humans demonstrated higher diversity between infection states than within them (Fig. S3). The t-statistic for the "All within infection" versus "All between infection" for the human
210 module was -150.82 and the p-value was also significant (Table S4) which confirmed our hypothesis.

Perturbation and resilience of the human URT microbiome is not dependent on the clinical parameters or influenza virus subtype

To complement the qualitative overview of the influenza-infected data points, we integrated additional
215 clinical metadata including gender, antibiotic usage, age and influenza subtype, as well as detailing the amplification of influenza genomes from these samples to more accurately classify these data points as either positive or unknown for the presence of virus. We tested if the positive and unknown infected

microbiomes were distinct enough to cluster separately based on their beta diversity. We analyzed the beta diversity metrics using PCoA, focusing just on the IAV-infected samples, however we could not derive any
220 conclusions from this analysis alone. The grouping of infected samples based on gender did not show any significant association (ANOSIM R=0.03124, p-value <0.023), implying that there was no significant effect of gender on the clustering of the samples (Table S5). Additionally, only 2.1% of the variation in the distances is explained when the gender of the patients is accounted for as a predictor of the model, using distances between the samples as the response variable (ADONIS *df* 1, R^2 =0.0209). Hence, sex could not
225 be correlated with the microbiome of the infected human samples. Additionally, age and effects of post visit antibiotic treatment on the microbiome trends were also examined. No significant association could be observed between post visit antibiotic usage and clustering of the infected human samples (ANOSIM R=-0.046, p-value < 0.732), which was surprising. However, the age of the patients seemed to have some influence on the sample grouping when all 26 categorical values were taken into consideration (ANOSIM
230 R=0.47, p-value < 0.001). The statistical analyses show that while the p-value is significant, the clustering on the basis of age is only moderately strong (ADONIS R^2 = 0.409, *df* 25). Since there was no indication of this effect among IAV-infected patients in the ordination plots, it is possible that the significant p-value could be attributed to the high number of samples or the differences in dispersion among the different sample groupings, emphasizing the importance of both the p-value and the effect size.

235

Pseudomonas **blooms during viral infection in the human URT**

We examined taxonomic profiles for all the infected and healthy patients across all the time points using the taxa abundance values for top ten most prevalent taxa at the order level (Fig. 4). All other taxa were pooled into an additional taxon named “Other”. *Pseudomonas* (orange) is the most abundant taxonomic
240 group in all influenza infection human samples (Fig. S5, Fig. 4), as was also observed in the ferrets. Less abundant phyla included *Bacteroidetes*, *Firmicutes*, *Actinobacteria* and some other families of *Proteobacteria*, like *Xanthomonadaceae* and *Pasteurellaceae* (c. *Gammaproteobacteria*) and *Brucellaceae* of the *Rhizobiales* order (c. *Alphaproteobacteria*). As for the uninfected subjects, *Actinobacteria* (yellow) is the most dominant taxon and *Pseudomonas* is the least abundant taxonomic group present. Other less

245 abundant phyla included *Verrucomicrobia* and within the *Proteobacteria*, the *Alphaproteobacteria* and *Epsilonproteobacteria* classes.

Distribution of the human URT microbiome into distinct ecostates due to IAV infection

The iDMM model was run over 2000 iterations over all data points (33 patients at multiple timepoints), which collapsed the data into a total of four ecostates (Table 3). Plotting the mean of the likelihood ratio at each
250 iteration showed that 25 iterations into the analysis, the maximum likelihood ratio converges for the model. One of the four ecostates included all 127 uninfected data points (or the "healthy" ecostate) while the 146 infected data points were distributed across the three other ecostates (or "unhealthy" ecostates). As was observed in the ferrets, a few patients moved from the "unhealthy" ecostates during acute influenza infection to the "healthy" ecostate in the later time points. This suggests the human microbiome also exhibits
255 resilience but potentially weaker elasticity; however, the clinical study lacks the precise temporal control of the ferret study.

The iDMM analysis predicted the diagnostic OTU for the healthy ecostate to be Otu000008 which belongs to the *Flavobacteria* class (*Cloacibacterium*), with a posterior predictive probability of 0.08, followed by Otu000010 (Corynebacterium_1) and Otu000013 (*Comamonadaceae*), belonging to the class
260 Actinobacteria and Betaproteobacteria, respectively (Table 3). For the "unhealthy" ecostates, Otu000003, Otu000004 and Otu000002 were diagnostic for Ecostate 1, 2 and 3 respectively (Table 3). Ecostate 1 had the largest number of infected data points (114), followed by Ecostate 3 (20) and Ecostate 2 (9). Otu000003 and Otu000002 belong to the *Pseudomonadaceae* family (the latter being an unclassified *Pseudomonadaceae*), with relatively high posterior probabilities associated with each of them (Table 3).
265 Otu000004 belonged to the *Actinobacteria* class and was the diagnostic OTU for Ecostate 2 with 9 infected data points. Like the ferret data, the diagnostic OTUs for all four ecostates for the human samples are also among the first ten most abundant OTUs for the data. The results from the random forest classification aligned with our diagnostic iDMM OTU prediction in the human subjects as well (Table S6). The analysis showed Otu000002 (*Pseudomonas*) to be the most predictive of the IAV infected samples, followed by
270 Otu000001 (*Rhizobiales*) and Otu000003 (*Pseudomonas*) with a maximum accuracy of 71%.

Discussion

This study describes taxonomic microbiome population dynamics in the upper respiratory tract of humans and ferrets during influenza virus infection. Given the unequivocal association between viral and bacterial co-infection and influenza disease severity, there is a pressing need to better understand how perturbation of the host microbiome correlates with viral infection, and potentially facilitates opportunistic co-infection. The nature of the sequencing approach, that is a loci-based population survey, means that we can address taxonomy-centric ecological principles of disturbance and resilience (Relman, 2012; Walker et al., 2004) in the URT microbiome. The results strongly suggest that the core URT microbiome is disturbed by IAV infection via indirect and uncharacterized processes, which may in turn facilitate the bacterial pathogen co-infections causing more hospitalizations and morbidity associated with IAV infection. Additionally, the results provide clear designs for studies explicitly examining mechanistic links between IAV and bacterial co-infection, along with the development of therapeutic treatments aimed at the microbiome as a community.

Without disturbance or perturbation, the URT microbiome was stable in both uninfected ferrets and humans. IAV does not directly infect any microbiome constituents, yet infection disturbs the healthy-state microbiome in both ferrets and humans in a statistically robust manner. The microbiomes of infected individuals or animals (unhealthy) are quite different from each other. In addition, unhealthy microbiomes are divergent from healthy microbiome and numerous community assemblies are possible in the unhealthy state. This is a clear demonstration of the Anna Karenina principle (Zaneveld et al., 2017), restated as “all healthy microbiomes are the same, while all unhealthy microbiomes are uniquely so.” This high diversity of unhealthy microbiomes during early stages of acute infection is consistent with earlier studies (Charlson et al., 2011) but extends it to an indirect disturbance. We propose that the disturbance of the healthy URT microbiome creates transient ecological niches for opportunistic bacterial pathogens. How viral infection induces a disturbance in the microbiome requires further experimentation. Nevertheless, the host antiviral response seems a likely cause, though this requires host and microbiome metatranscriptomics or metaproteomics in controlled experiments focused at the onset of infection. Maximum disturbance is shown to be correlated with maximum viral loads and weight loss in the ferret model, which suggests a close relationship between infection, disease and disturbance of the microbiome, with kinetics that are similar to the antiviral response induced during IAV infection.

300 The sole statistical exception to the high community diversity of infected microbiomes was the increased relative abundance of *Pseudomonadales*, regardless of age, sex, antibiotic treatment, or even host organism. Oddly enough in humans, no significant influence of the host type (age and sex) or behavior (antibiotic usage) was observed on the temporal nature of the microbiome elasticity, and more statistical power would be needed to draw any more robust associations from the data. Yet, the "bloom" of
305 *Pseudomonadales* is consistent with previous reports in H1N1-infected patients (Chaban et al., 2013; Klein et al., 2016; Leung et al., 2013; Tarabichi et al., 2015). In our study, *Pseudomonadales* are present in relatively low proportions in the healthy microbiome of these host organisms. The "bloom" might be due to a more hostile environment for the other taxa or perhaps a more hospitable environment for the *Pseudomonadales,* making this an excellent candidate for future transcriptional profiling. Moreover, the
310 increased abundance of *Pseudomonadales* and the decreased relative abundance of *Clostridiales* in the infected cohort suggest a potential use for probiotic treatments capable of modulating the microbiome back into the healthy ecostate (Chen et al., 2016). Such a treatment would be homologous to those proposed for perturbing or restoring the gut microbiome (Spinler et al., 2014). Understanding how and why *Pseudomonadales* succeed after disturbance will provide valuable information for conducting future
315 microbiome centric URT studies in a controlled setting. It should be noted the blooming *Pseudomonads* are not *P. aeruginosa*, instead a variety of other related families and genera, and understanding their functional potential and role requires shotgun metagenomics analyses.

In the ferret model, there is a clear demonstration of ecological resilience in the URT microbiome; namely a return to the original community after disturbance, a phenomenon also observed, albeit less clearly, in
320 the human samples. Similar observations have been reported in the human gut microbiome after the massive disturbance associated with antibiotic treatment (Relman, 2012), though our findings expands it to the URT and the indirect effects of the IAV infection. The controlled experiments with ferrets resulted in near complete recovery. Human URT microbiomes do not unequivocally show a return to the health state, but in several patients, the microbiome returned to the healthy ecostate. Although it is tempting to suggest
325 that the ferret microbiome might have greater elasticity (i.e. less time required for demonstration of resilience), there are multiple potential reasons for the discrepancy between ferrets and humans. Considering metabolic rate relative to organism size, the ferret may recover at a more rapid rate simply due

to a higher metabolism. Moreover, immunological imprinting could potentially contribute to this discrepancy, given that the ferrets used in the study have never been exposed to influenza before. The same cannot be
330 assumed for the human subjects, which are bound to have some levels of to pre-existing immunity to the virus with impact on the IAV induced cellular and adaptive responses. More pertinently, the human cohort has an undetermined infection date and a selection bias towards phenotypically responsive patients, in that the zero time (Day 0) is the first hospital visit. Beyond the potential differences in absolute temporal trends in microbiome resilience and elasticity, the ferret and human microbiomes share similar trends at the
335 ecosystem and individual taxon level that warrant further experimentation. The results here provide an experimental baseline for examining both predictive and therapeutic intervention focused experiments in the ferret model system. For example, the presented hypothesis that IAV driven microbiome disturbance increases the propensity for bacterial pathogen co-infection can be robustly tested by bi-partite exposures to viral, and then bacterial pathogens. The effects of lifestyle (diet, smoking, exercise) and abiotic influences
340 (humidity, temperature) on the microbiome and its resilience should also be examined, particularly with regards to temporal dynamics of microbiome disturbance and recovery. Therapeutic approaches involve thwarting the associated threat of an opportunistic bacterial pathogen or interventions focused on the bloom of *Pseudomonas.* Our results are especially relevant in the context of secondary bacterial infections following primary infection with IAV (Sharma-Chawla et al., 2016). Multiple studies, including this one, have
345 now shown that a subset of the taxa that are most frequently associated with secondary infections have increased relative abundance during IAV infection. It is possible that such outcomes could be reduced by modulating the host immune response during IAV infection (Wang et al., 2013). Reducing the high morbidity and mortality rates associated with such secondary infections would improve quality of life and longevity while simultaneously reducing healthcare costs (Gupta et al., 2008; Kash and Taubenberger, 2015; Morris
350 et al., 2017).

Acknowledgements

The authors would like to thank research nurse Claudia Marco and the following clinical fellows and pediatricians that contributed to the recruitment of patients and the collection of samples used in this study: Marta Aravena, Catalina Gutierrez, Tania Lopez, Regina Perez and Cecilia Vizcaya from the Department
355 of Pediatric Infectious Diseases and Immunology, Facultad de Medicina, Pontificia Universidad Católica de

Chile, Santiago, Chile. This project has been partly funded with federal funds from the National Institute of Allergy and Infectious Diseases, National Institutes of Health, Department of Health and Human Services under Contract Number HHNS272200900007C/ HHSN266200700010C and Grant Number U19AI110819, grants from the Comisión Nacional de Investigación Científica y Tecnológica (FONDECYT 1121172 and 1161791 to R.A.M.; and PIA ACT 1408 to R.A.M. and M.F.), and the Chilean Ministry of Economy, Development and Tourism (P09/016-F to R.A.M.). This study was also partially supported by CRIP (Center for Research in Influenza Pathogenesis), an NIAID funded Center of Excellence for Influenza Research and Surveillance (CEIRS, contract # HHSN272201400008C) and by NIAID grant U19AI135972 (to A.G.-S. and R.A.M.).

Author Contributions

D.K. and R.R. analyzed data, prepared illustrations, and wrote the manuscript. M.F. designed human cohort study, recruited patients, collected clinical metadata and wrote parts of the paper. G.S.T., B.E.P. carried out data analysis and wrote parts of the paper. A.B. carried out data analysis, prepared illustrations, and wrote parts of the paper. D.W. and B.M. obtained funding, designed and supervised experiments and analyzed data. S.D. supervised experiments and analyzed data. I.B. recruited patients and collected clinical metadata. R.H. performed sequencing experiments and metadata compilation. M.S., I.M., R.A.A. performed ferret experiments. I.S. performed data processing and analysis. K.E.N. Obtained funding, supervised this study and wrote parts of the paper. A.G.S. conceived and supervised this study and wrote the manuscript. C.L.D. supervised this study, designed informatics analyses, analyzed data, prepared illustrations, and wrote the manuscript. R.A.M. obtained funding, conceived and supervised this study, designed and performed experiments, analyzed data, prepared illustrations, and wrote the manuscript.

Declaration of Interests

The authors declare no competing interests.

Figures

Figure 1: Diversity of the URT microbiome in ferrets during IAV infection. Beta diversity analysis for longitudinal URT samples taken after experimental infection with the A/Netherlands/602/09 H1N1 strain (Infected) or in control animals. Principal coordinates analysis (PCoA) of Bray Curtis distances was performed for all samples. Data points for uninfected ferrets are in blue, the T=0 for the infected ferrets in lavender, the T=14 for infected ferrets in cyan, and all other infected time points are in red. The total variability explained by all three principal coordinates (PCs) is shown on the axes. Each group of ferret was composed of 7 animals.

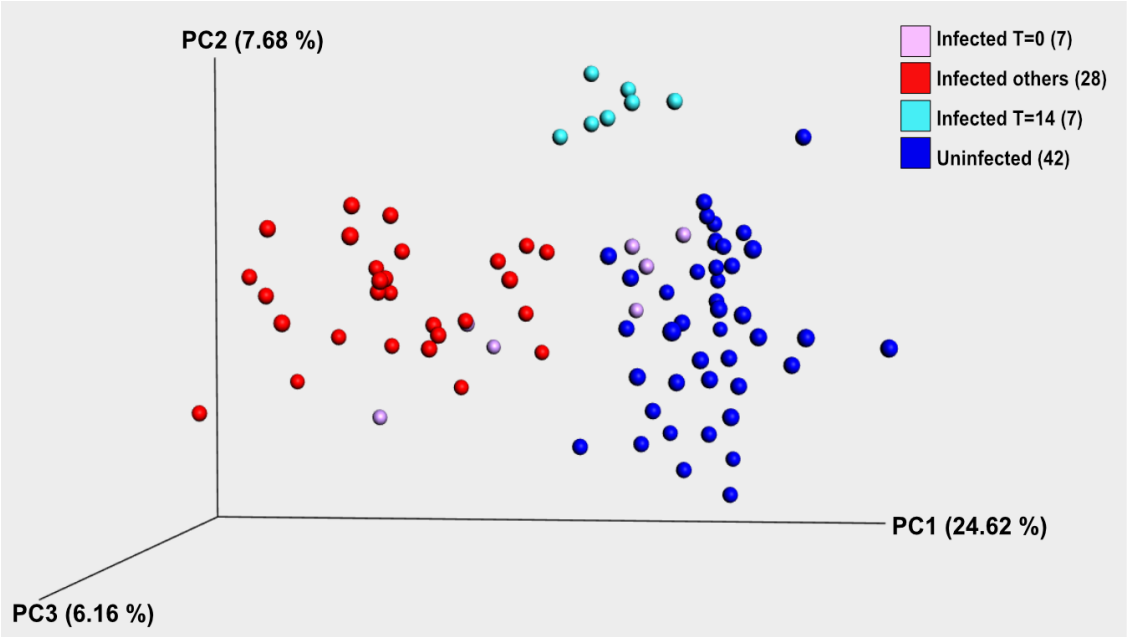

Figure 2. Qualitative and quantitative representation of the temporal trajectory of the ferret microbiome. (A) Percent body weights of groups of 7 ferrets mock inoculated (uninfected) or intranasally infected with $1X10^6$ pfu of influenza A/Neth/602/09 virus. Body weights were determined daily for 14 days, and are represented as the average percent body weight compared to the initial weight of each animal on the day of inoculation and error bars are the standard deviation for each time point. (B) Viral titers of nasal washes of ferrets infected with $1X10^6$ pfu of A/Neth/602/09 virus. Nasal washes were obtained on days 1, 3, 5 and 7 post infection and are represented as the average viral titer of 7 infected animals. Error bars indicate the standard deviation for each time point. (C-D) Comprehensive taxonomic breakdown of an influenza infected (C) and uninfected ferret (D), at different timepoints. Taxa abundance values for top ten most prevalent taxa at the order level for different timepoints (0 to14 dpi). Only taxa labels with a confidence score of >= 90% were retained in the analysis. The remaining taxa are pooled into an additional taxon labeled "Other". (E-F) Average and standard deviation of the relative *Pseudomonas* abundance across all infected (E) and uninfected (F) ferrets (n=7 for each).

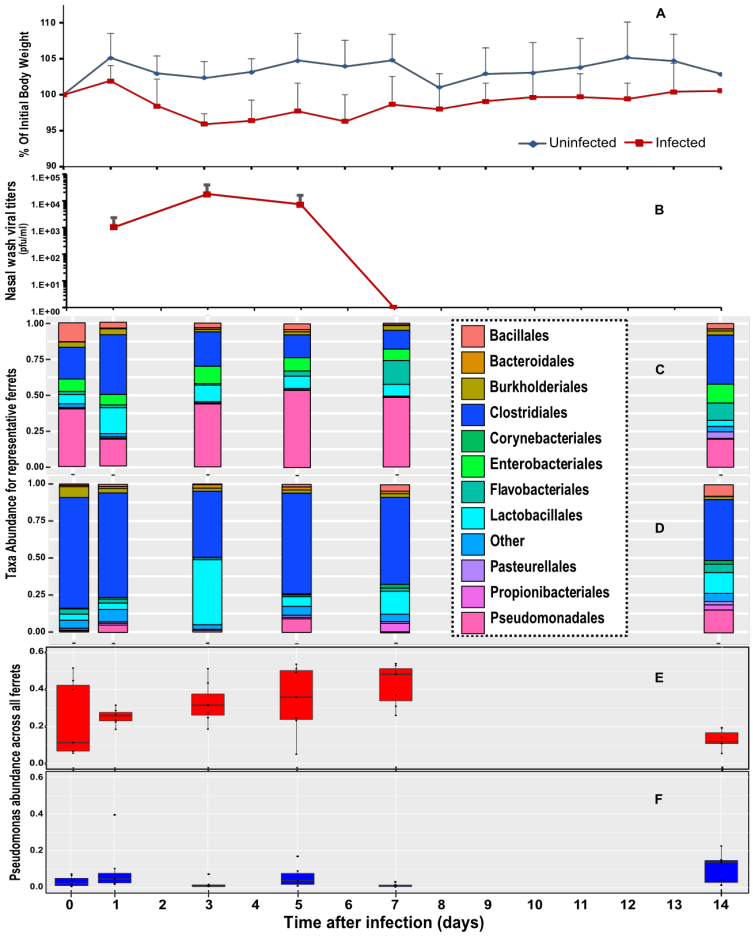

Figure 3. Diversity of the URT microbiome of human patients infected with IAV. Beta diversity analysis for longitudinal nasopharyngeal swab samples obtained from heathy and IAV infected individuals. Principal coordinates analysis (PCoA) of Bray Curtis distances was done for samples from humans, labeled as influenza positive in red (P), influenza unknown in yellow (U) and uninfected samples in blue (Flu negative). The total variability explained by all three principal coordinates (PCs) is shown on the axes.

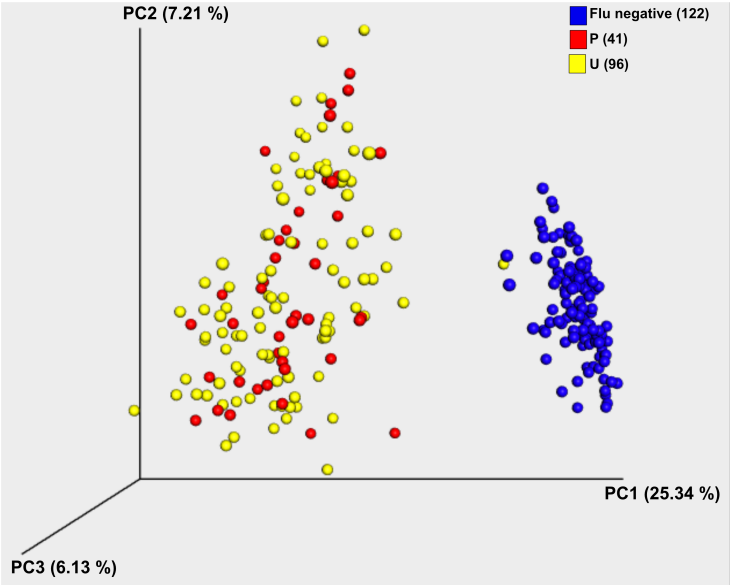

Figure 4. Comprehensive taxonomic breakdown for IAV-free (left) and IAV-infected (right) human subjects. The plot summarizes the relative taxonomic abundances at the class level for taxonomic groups that are present in greater than 5% of the samples (see legend below). Gammaproteobacteria (*Pseudomonas*) bloom is prevalent among the infected patients (right), whereas Actinobacteria is the most abundant among healthy patients.

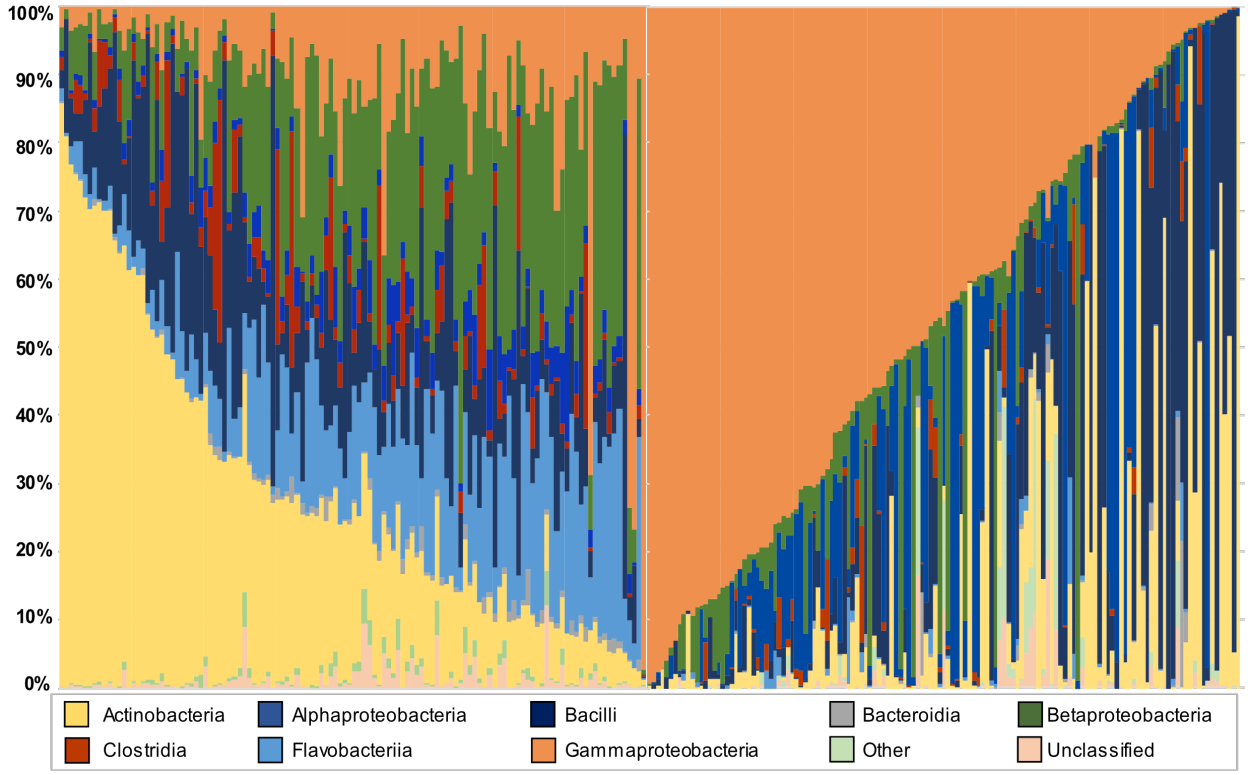

TABLES

TABLE 1. Summary statistics for amplicon-based sequencing of the V1-V3 region of the 16S rRNA gene

	Ferrets	**Humans**
Total no. of samples[a]	86	273
Influenza negative subjects	7	22
Influenza positive subjects	7	33
Total no. of reads	649 440	2 342 992
Total no. of OTUs	259	707
No. of reads mapped to OTUs	514 099 (79.2%)	2 151 233 (91.8%)

465

a. All ferret and human samples were extracted from nasal washes and the nasopharyngeal swabs, respectively, at several timepoints post infection.

TABLE 2. Diagnostic microbes for each ecostate from the 1000th iteration of the iDMM model for the ferret samples. Number of iterations depends on the total number of samples (84) present in the data. All later timepoint ferrets (T14) return to the healthy ecostate (1)

470

Ecostate	**Total samples**	**No. of samples[a]**			**Diagnostic OTU**	**Probability associated[b]**	**Taxonomy**
		T14	**[T7 + T5 + T3 + T1]**	**T0**			
1 (Healthy)	**58** (42)	**14** (7)	**33** (28)	**11** (7)	Otu000001	0.1865749	Clostridia; Peptostreptococcacea
2 (Infected)	**26** (42)	**0** (7)	**23** (28)	**3** (7)	Otu000004	0.1112045	Pseudomonadales; Moraxellaceae; Acinetobacter

a. No. of samples at final iteration for each timepoint in bold (original starting values in parentheses).
b. Bayesian posterior predictive probabilities associated with the microbe which is the highest probability for that ecostate.

475

TABLE 3. Diagnostic microbes for each ecostate from the 2000th iteration of the iDMM model for the infected and uninfected humans. Number of iterations depends on the number of samples (273) present in the data.

Ecostate	Final distribution[a]	Original sample distribution[b]	Diagnostic OTU	Probability associated[c]	Taxonomy
1 + 2 + 3 (Infected)	114	146	Otu000003	0.361568	Gammaproteobacteria; Pseudomonas
	9		Otu000004	0.4989514	Actinobacteria; Corynebacteriu
	20		Otu000002	0.01584407	Gammaproteobacteria; Pseudomonas
4 (Healthy)	130	127	Otu000008	0.07636954	Flavobacteria; Cloacibacteriur

a. Distribution of samples within ecostates after running the iDMM model.
b. Distribution of samples before running the iDMM model.
c. Bayesian posterior predictive probabilities associated with the diagnostic microbe which is the highest probability for that ecostate.

480

485

490

Materials and Methods

495 **Human sample collection and study design**

Patient clinical–epidemiological data, along with nasopharyngeal swabs were collected after informed written consent was obtained under protocol 11-116, reviewed and approved by the Scientific Ethics Committee of the School of Medicine at Pontificia Universidad Catolica de Chile (PUC) before the start of sample collection. Between July 2011 and November 2012, a total of 146 nasopharyngeal swabs samples
500 were collected from 30 hospitalized patients in Santiago, Chile, diagnosed with influenza-like illness (ILI). Of the 30 patients in the study, 28 were confirmed and subtyped as H1N1pdm09 or H3N2 Influenza through RT-PCR by Clinical Virology Laboratory at PUC. The remaining 2 patients could not be confirmed as influenza positive by qRT-PCR, RT-PCR and/or the hemagglutination inhibition (HI) assay, but still displayed the perturbation in their microbiome so they were included in the analyses. Between one and six
505 samples from the acute phase of infection were taken from each patient, together with a sample up to 22 days post diagnosis (convalescence phase or healthy baseline) from most of individuals. Control samples from 22 healthy individuals, confirmed as negative against influenza A virus and 13 other common respiratory viruses, were taken with the same criteria in March to June of 2014. Epidemiological history, signs and symptoms, other diagnostics and treatments of each patient were also collected during
510 hospitalization as detailed in Table S3. Furthermore, 96.4% of patients received oseltamivir antiviral treatment and 89.3% received antibiotics originating from the families of the fluoroquinolones (levofloxacine, morifloxacine or ciprofloxacine), 3rd generation cephalosporins (ceftriaxone or cefepime), carbapenems (meropenem or imipenem), metrodinazole, cotrimoxazole or vancomycin. These treatments where supplied in a combination of 5 (4% of patients), 4 (8%), 3 (12%), 2 (40%) or one (36%) antibiotics in
515 a complete treatment (at least seven days) or less. Severe infection criteria were established in accordance with the hospitalization due to influenza and/or derivation to Critical Care Unit (which involves oxygen support or mechanical ventilation and/or vasoactive drug administration) after symptoms onset. The microbiome data analyzed were obtained from the nasopharyngeal swabs of 33 infected subjects (14 male and 19 female), ages ranging from one year to 76 years, for a total of 146 samples. The naming convention
520 of influenza A viruses detected from patients are as follows: A/Santiago/p*x*d*y*/2011 or A/Santiago/p*x*d*y*/2012 (p=patient and d=day). The negative controls analyzed in the study were

nasopharyngeal swabs taken from 22 healthy patients (10 males and 12 females), most taken at all 6 time points (1, 2, 3, 5, 8 and 28 dpi), for a total of 127 samples, which were negative for influenza and other respiratory infections.

525

Ferret infection and sample collection

The animal experiments described here were performed under protocols approved by the Icahn School of Medicine at Mount Sinai Institutional Animal Care and Use Committee. All Infections and nasal wash samples were done on ferrets anesthetized with ketamine (25 mg/kg) and xylazine (2mg/kg)
530 intramuscularly. A detailed time point study was conducted in ferrets infected with $1x10^6$ plaque forming units per animal of the A/Netherlands/602/2009 H1N1 pandemic strain through intranasal inoculation, and then nasal wash samples were taken from 7 uninfected and 7 infected animals. To study the effect of IAV infection on the URT microbiome, samples were taken at 6 different timepoints: on day 0 and then on days 1, 3, 5, 7 and 14 post infection (dpi). Body weights were obtained for 14 consecutive days, and viral
535 titers were determined by plaque assay in MDCK cells as previously described (Manicassamy et al., 2010) for the first 7 dpi.

Sample processing and sequence analyses

All bacterial genomic DNA (gDNA) extractions were performed using the Qiagen All Prep kit and were
540 subjected to 16S amplification using the HMP 16S sequencing protocol and the amplicons were sequenced using the Roche 454 Titanium pipeline (Margulies et al., 2005). Appropriate positive and negative controls from amplification were also included. The V1-V3 hypervariable regions were amplified for 16S profiling (forward primer: 27F 5'- AGAGTTTGATCCTGGCTCAG-3' and reverse primer: 534R 5'-ATTACCGCGGCTGCTGG-3') of the 16S ribosomal RNA gene.

545

Data Analysis

Reads were de-multiplexed according to barcodes followed by trimming of both barcodes and adapter sequences. Following the initial processing of the sequence data, sequences were combined, dereplicated and aligned in mothur (version 1.36.1 (Schloss et al., 2009)) using the SILVA template (Quast et al., 2013)

550 (SSURef_NR99_123) and the sequences were organized into clusters of representative sequences based on taxonomy called Operational Taxonomic Units (OTU) using the UPARSE pipeline (Edgar, 2013). In the ferrets, all except two libraries generated more than 3000 reads per sample. A total of 649,440 sequences were subsequently clustered into 259 OTUs with a sequence similarity threshold of 97% (Schloss et al., 2009), a length threshold of 250 bp and an expected error threshold of 0.15. For human samples, the
555 distribution of reads per sample was much more uneven. A total of 2,342,992 sequences were sorted into 707 OTUs, using the same thresholds as above and the same downstream filtering of the OTUs and samples was performed in a similar manner.

Initial filtering of the samples ensured discarding samples containing less than 5 sequences. Libraries were normalized using metagenomeSeq's cumulative sum scaling method (Paulson et al., 2013) to account for
560 library size acting as a confounding factor for the beta diversity analysis. Moreover, in addition to discarding singletons, OTUs that were observed fewer than 5 times in the count data were also filtered out to avoid the inflation of any contaminants that might skew the diversity estimates.

Informatics

Beta diversity metrics were calculated across all samples using the Bray-Curtis dissimilarity index and
565 overall trends in the community composition for ferrets and humans on the basis of presence or absence of the flu infection were explored using Principal Coordinates Analysis (PCoA) in QIIME (Caporaso et al., 2010) (version 1.9.1) and then visualized in Emperor (Vazquez-Baeza et al., 2013)(version 0.9.51).

Taxonomic classification of the samples was done by classifying the representative sequences from the OTUs using mothur and the SILVA database, with a confidence threshold of 97%. The relative abundances
570 for the taxonomic profiles for each subject was calculated in QIIME using summarize_taxa.py. The visualization of the top ten most prevalent taxa for each of the organisms was done in R (version 3.2.2) using dplyr and reshape2 to manipulate the data and ggplot2 for generating the plots. Following the qualitative analysis of the data, we employed an infinite dimensional generalization of the multinomial Dirichlet mixture model (O'Brien et al., 2016) which tries to model the original set of communities from the
575 input data with additional posterior predictive probabilities (PPD) for statistical cut offs. The model was executed over 1000 iterations for the ferret data and 2000 iterations for the human data since this parameter should increase with the number of samples present in the dataset. Scripts located at

https://github.com/jacobian1980/ecostates were improved by introducing a seed in the beginning of the algorithm to improve the reproducibility of the model and optimized the community number based on the PPDs which compare empirically observed data with the data that would be expected if the DMM were the correct underlying model (Gelman et al., 1996; Meng, 1994). All downstream analyses with the communities, including exploration of community membership, were performed in R. Additionally, a diagnostic OTU was computed for each ecostate, or sampled community, which is the OTU with the highest posterior predictive probability in the ecostate and therefore drives the clustering. The quantitative portion of the analysis was supplemented by performing random forest classification on the data to confirm the diagnostic results using Scikit-Learn (version 0.18.1) in Python (version 3.5.2) from Continuum Analytics Anaconda Suite. The training dataset included: a *(n x m)*-dimensional attribute matrix consisting of the relative abundance values for the OTUs and the samples, where n and m refer to the number of samples and the number of OTUs respectively, and a (*n)*-dimensional vector relating each observation to the 2 experimental states (positive and negative for the virus). The average of the feature importance vectors from 20000 models that could accurately predict all 5 left-out samples (~85% accuracy) was computed to obtain a weight for each OTU's predictive capacity to classify the experimental state of each sample. The hyperparameters for the random forest model were 618 decision trees per forest, gini index as impurity criterion and the square root of the number of features (OTUs in this case) to use for each split in the decision tree.

Data Availability

Raw amplicon sequence reads for this study have been deposited to Sequence Read Archive (SRA) under accession number: SRP009696 [BioProject accession number: PRJNA76689] for the ferrets and accession numbers: SRP092459 [BioProject accession number: PRJNA240559] and SRP128464 [PRJNA240562] for the infected and uninfected human subjects respectively.

605 **References**

Belser, J.A., Eckert, A.M., Tumpey, T.M., and Maines, T.R. (2016). Complexities in Ferret Influenza Virus Pathogenesis and Transmission Models. Microbiology and molecular biology reviews : MMBR *80*, 733-744.

610 Belser, J.A., Katz, J.M., and Tumpey, T.M. (2011). The ferret as a model organism to study influenza A virus infection. Disease Models & Mechanisms *4*, 575-579.

Blyth, C.C., Webb, S.A., Kok, J., Dwyer, D.E., van Hal, S.J., Foo, H., Ginn, A.N., Kesson, A.M., Seppelt, I., Iredell, J.R.*, et al.* (2013). The impact of bacterial and viral co-infection in severe influenza. Influenza Other Respir Viruses *7*, 168-176.

615 Brundage, J.F. (2006). Interactions between influenza and bacterial respiratory pathogens: implications for pandemic preparedness. Lancet Infect Dis *6*, 303-312.

Brundage, J.F., and Shanks, G.D. (2008). Deaths from bacterial pneumonia during 1918-19 influenza pandemic. Emerg Infect Dis *14*, 1193-1199.

Caporaso, J.G., Kuczynski, J., Stombaugh, J., Bittinger, K., Bushman, F.D., Costello, E.K., Fierer, N., Pena,
620 A.G., Goodrich, J.K., Gordon, J.I.*, et al.* (2010). QIIME allows analysis of high-throughput community sequencing data. Nat Methods *7*, 335-336.

Chaban, B., Albert, A., Links, M.G., Gardy, J., Tang, P., and Hill, J.E. (2013). Characterization of the upper respiratory tract microbiomes of patients with pandemic H1N1 influenza. PLoS One *8*, e69559.

Charlson, E.S., Bittinger, K., Haas, A.R., Fitzgerald, A.S., Frank, I., Yadav, A., Bushman, F.D., and Collman,
625 R.G. (2011). Topographical continuity of bacterial populations in the healthy human respiratory tract. Am J Respir Crit Care Med *184*, 957-963.

Chen, H.W., Liu, P.F., Liu, Y.T., Kuo, S., Zhang, X.Q., Schooley, R.T., Rohde, H., Gallo, R.L., and Huang, C.M. (2016). Nasal commensal Staphylococcus epidermidis counteracts influenza virus. Sci Rep *6*, 27870.

Edgar, R.C. (2013). UPARSE: highly accurate OTU sequences from microbial amplicon reads. Nat
630 Methods *10*, 996-998.

Gao, Z., Kang, Y., Yu, J., and Ren, L. (2014). Human pharyngeal microbiome may play a protective role in respiratory tract infections. Genomics Proteomics Bioinformatics *12*, 144-150.

Gelman, A., Meng, X.-L., and Stern, H. (1996). POSTERIOR PREDICTIVE ASSESSMENT OF MODEL FITNESS VIA REALIZED DISCREPANCIES. Statistica Sinica *6*, 733-760.

635 Gupta, R.K., George, R., and Nguyen-Van-Tam, J.S. (2008). Bacterial pneumonia and pandemic influenza planning. Emerg Infect Dis *14*, 1187-1192.

Holmes, I., Harris, K., and Quince, C. (2012). Dirichlet Multinomial Mixtures: Generative Models for Microbial Metagenomics. PLOS ONE *7*, e30126.

Huang, Y.J., and Lynch, S.V. (2011). The emerging relationship between the airway microbiota and
640 chronic respiratory disease: clinical implications. Expert Rev Respir Med *5*, 809-821.

Ichinohe, T., Pang, I.K., Kumamoto, Y., Peaper, D.R., Ho, J.H., Murray, T.S., and Iwasaki, A. (2011). Microbiota regulates immune defense against respiratory tract influenza A virus infection. Proc Natl Acad Sci U S A *108*, 5354-5359.

Iuliano, A.D., Roguski, K.M., Chang, H.H., Muscatello, D.J., Palekar, R., Tempia, S., Cohen, C., Gran, J.M.,
645 Schanzer, D., Cowling, B.J.*, et al.* (2017). Estimates of global seasonal influenza-associated respiratory mortality: a modelling study. Lancet.

Johnson, N.P., and Mueller, J. (2002). Updating the accounts: global mortality of the 1918-1920 "Spanish" influenza pandemic. Bulletin of the history of medicine *76*, 105-115.

Kash, J.C., and Taubenberger, J.K. (2015). The role of viral, host, and secondary bacterial factors in
650 influenza pathogenesis. Am J Pathol *185*, 1528-1536.

Klein, E.Y., Monteforte, B., Gupta, A., Jiang, W., May, L., Hsieh, Y.H., and Dugas, A. (2016). The frequency of influenza and bacterial coinfection: a systematic review and meta-analysis. Influenza Other Respir Viruses *10*, 394-403.
Langevin, S., Pichon, M., Smith, E., Morrison, J., Bent, Z., Green, R., Baker, K., Solberg, O., Gillet, Y., Javouhey, E.*, et al.* (2017). Early nasopharyngeal microbial signature associated with severe influenza in children: a retrospective pilot study. J Gen Virol.
Leung, R.K., Zhou, J.W., Guan, W., Li, S.K., Yang, Z.F., and Tsui, S.K. (2013). Modulation of potential respiratory pathogens by pH1N1 viral infection. Clin Microbiol Infect *19*, 930-935.
Manicassamy, B., Medina, R.A., Hai, R., Tsibane, T., Stertz, S., Nistal-Villan, E., Palese, P., Basler, C.F., and Garcia-Sastre, A. (2010). Protection of mice against lethal challenge with 2009 H1N1 influenza A virus by 1918-like and classical swine H1N1 based vaccines. PLoS Pathog *6*, e1000745.
Margulies, M., Egholm, M., Altman, W.E., Attiya, S., Bader, J.S., Bemben, L.A., Berka, J., Braverman, M.S., Chen, Y.J., Chen, Z.*, et al.* (2005). Genome sequencing in microfabricated high-density picolitre reactors. Nature *437*, 376-380.
Meng, X.-L. (1994). Multiple-Imputation Inferences with Uncongenial Sources of Input. Statist Sci *9*, 538-558.
Morens, D.M., Taubenberger, J.K., and Fauci, A.S. (2008). Predominant role of bacterial pneumonia as a cause of death in pandemic influenza: implications for pandemic influenza preparedness. J Infect Dis *198*, 962-970.
Morris, D.E., Cleary, D.W., and Clarke, S.C. (2017). Secondary Bacterial Infections Associated with Influenza Pandemics. Front Microbiol *8*, 1041.
O'Brien, J.D., Record, N., and Countway, P. (2016). The power and pitfalls of Dirichlet-multinomial mixture models for ecological count data. bioRxiv.
Paulson, J.N., Stine, O.C., Bravo, H.C., and Pop, M. (2013). Differential abundance analysis for microbial marker-gene surveys. Nature Methods *10*, 1200.
Planet, P.J., Parker, D., Cohen, T.S., Smith, H., Leon, J.D., Ryan, C., Hammer, T.J., Fierer, N., Chen, E.I., and Prince, A.S. (2016). Lambda Interferon Restructures the Nasal Microbiome and Increases Susceptibility to Staphylococcus aureus Superinfection. MBio *7*, e01939-01915.
Quast, C., Pruesse, E., Yilmaz, P., Gerken, J., Schweer, T., Yarza, P., Peplies, J., and Glockner, F.O. (2013). The SILVA ribosomal RNA gene database project: improved data processing and web-based tools. Nucleic Acids Res *41*, D590-596.
Relman, D.A. (2012). The human microbiome: ecosystem resilience and health. Nutrition reviews *70*, S2-S9.
Schloss, P.D., Westcott, S.L., Ryabin, T., Hall, J.R., Hartmann, M., Hollister, E.B., Lesniewski, R.A., Oakley, B.B., Parks, D.H., Robinson, C.J.*, et al.* (2009). Introducing mothur: open-source, platform-independent, community-supported software for describing and comparing microbial communities. Appl Environ Microbiol *75*, 7537-7541.
Shah, N.S., Greenberg, J.A., McNulty, M.C., Gregg, K.S., Riddell, J.t., Mangino, J.E., Weber, D.M., Hebert, C.L., Marzec, N.S., Barron, M.A.*, et al.* (2016). Bacterial and viral co-infections complicating severe influenza: Incidence and impact among 507 U.S. patients, 2013-14. J Clin Virol *80*, 12-19.
Sharma-Chawla, N., Sender, V., Kershaw, O., Gruber, A.D., Volckmar, J., Henriques-Normark, B., Stegemann-Koniszewski, S., and Bruder, D. (2016). Influenza A Virus Infection Predisposes Hosts to Secondary Infection with Different Streptococcus pneumoniae Serotypes with Similar Outcome but Serotype-Specific Manifestation. Infect Immun *84*, 3445-3457.
Spinler, J.K., Sontakke, A., Hollister, E.B., Venable, S.F., Oh, P.L., Balderas, M.A., Saulnier, D.M., Mistretta, T.A., Devaraj, S., Walter, J.*, et al.* (2014). From prediction to function using evolutionary genomics: human-specific ecotypes of Lactobacillus reuteri have diverse probiotic functions. Genome Biol Evol *6*, 1772-1789.

Tarabichi, Y., Li, K., Hu, S., Nguyen, C., Wang, X., Elashoff, D., Saira, K., Frank, B., Bihan, M., Ghedin, E.*, et al.* (2015). The administration of intranasal live attenuated influenza vaccine induces changes in the nasal microbiota and nasal epithelium gene expression profiles. Microbiome *3*, 74.
Vazquez-Baeza, Y., Pirrung, M., Gonzalez, A., and Knight, R. (2013). EMPeror: a tool for visualizing high-throughput microbial community data. Gigascience *2*, 16.
Walker, B., Holling, C.S., Carpenter, S.R., and Kinzig, A. (2004). Resilience, adaptability, and transformability in social-ecological systems. Ecology and Society *9*, 5.
Wang, J., Li, F., Sun, R., Gao, X., Wei, H., Li, L.J., and Tian, Z. (2013). Bacterial colonization dampens influenza-mediated acute lung injury via induction of M2 alveolar macrophages. Nat Commun *4*, 2106.
Whelan, F.J., Verschoor, C.P., Stearns, J.C., Rossi, L., Luinstra, K., Loeb, M., Smieja, M., Johnstone, J., Surette, M.G., and Bowdish, D.M. (2014). The loss of topography in the microbial communities of the upper respiratory tract in the elderly. Ann Am Thorac Soc *11*, 513-521.
Wu, S., Jiang, Z.Y., Sun, Y.F., Yu, B., Chen, J., Dai, C.Q., Wu, X.L., Tang, X.L., and Chen, X.Y. (2013). Microbiota regulates the TLR7 signaling pathway against respiratory tract influenza A virus infection. Curr Microbiol *67*, 414-422.
Zaneveld, J.R., McMinds, R., and Vega Thurber, R. (2017). Stress and stability: applying the Anna Karenina principle to animal microbiomes. Nature Microbiology *2*, 17121.